Graphullerite: A Thermally Conductive and Remarkably Ductile Allotrope of Polymerized Carbon

Connor Jaymes Dionne, Muhammad Akif Rahman, and Ashutosh Giri*

Read Online

ACCESS | Metrics & More | Article Recommendations | Supporting Information

ABSTRACT: The understanding of the fundamental relationships between chemical bonding and material properties, especially for carbon allotropes with diverse orbital hybridizations, is significant from both scientific and applicative standpoints. Here, we elucidate the influence of the intermolecular covalent bond configuration on the mechanical and thermal properties of polymerized fullerenes by performing systematic atomistic simulations on graphullerite, a newly synthesized crystalline polymer of C_{60} with a hexagonal lattice similar to that of graphene. Specifically, we show that the polymerization of C_{60} molecules into two-dimensional sheets (and three-dimensional layered structures) offers tunable control over their mechanical and thermal properties via the replacement of weak intermolecular van der Waals interactions between the fullerene molecules with strong sp^3 covalent bonds. More specifically, we show that graphullerite possesses highly anisotropic mechanical as well as thermal properties resulting from the variation in the chemical bonding configuration along the different directions. In terms of their mechanical properties, we find that graphullerite can be remarkably ductile if strained along a certain direction with oriented double bonds connecting the fullerenes. Combined with their drastically reduced Young's modulus and bulk modulus as compared to graphite, these materials have the potential to be utilized in flexible electronics and advanced battery electrode applications. In terms of their thermal properties, we show that the bonding orientation dictates the intrinsic phonon scattering mechanisms, which ultimately dictates their anisotropic temperature-dependent thermal conductivities. Taken together, their flexible nature combined with their remarkably high thermal conductivities as polymeric materials positions them as ideal candidates for a plethora of applications such as for the next generation of battery electrodes.
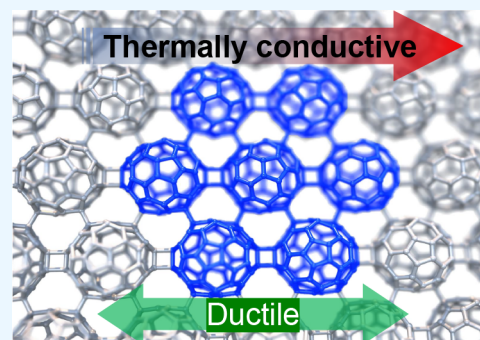
INTRODUCTION

Carbon, the element that provides the basis for life, and its synthetic allotropes are not only making significant contributions to our current technology, but are also redefining some of our fundamental understanding of materials science. For example, in the past few decades, graphene—an infinite two-dimensional (2D) sheet of a polymerized carbon allotrope (Figure 1a)—has become one of the most widely studied materials owing to its unique physical properties. Another widely studied allotrope of carbon is the C_{60} fullerene, which is effectively zero-dimensional, where the sp^2 carbon atoms polymerize without any termini (Figure 1b). More recently, by mixing sp^2- and sp^3-hybridized carbon atoms, extended networks of 2D carbon allotropes, dubbed graphullerene (Figure 1c), have been polymerized to form purely carbon-based macroscopic crystals capable of mechanical exfoliation.[1] The atomic structure of graphullerene constitutes fullerene subunits that are arranged in a hexagonal pattern (much like the infinite 2D sheet of graphene) and interconnected via sp^3 bonds, forming layers arranged in three-dimensional (3D) van der Waals solid (dubbed graphullerite).[1] Herein, we study the mechanical and thermal properties of these recently discovered

materials via reactive molecular dynamics (MD) simulations to reveal their unique anisotropic physical properties.

In general, carbon allotropes possess superior physical properties that mainly arise from the strong carbon−carbon bonds. For instance, graphene is endowed with metal-like electronic conductivity,[2,3] an extremely high Young's modulus ($\sim$1 TPa),[4] and one of the highest thermal conductivities ever measured (in excess of $\sim$5000 W m^{-1} K^{-1}).[5] Likewise, in the case of fullerite, which is a 3D bulk structure of C_{60} molecules, even though the molecules are held together by weaker van der Waals interactions, they are accompanied by several remarkable physical properties.[6−11] For example, the fullerite structure has been theorized as being among the least compressible materials,[12] as well as possessing a wide band gap with an electrical resistance that can be tuned via
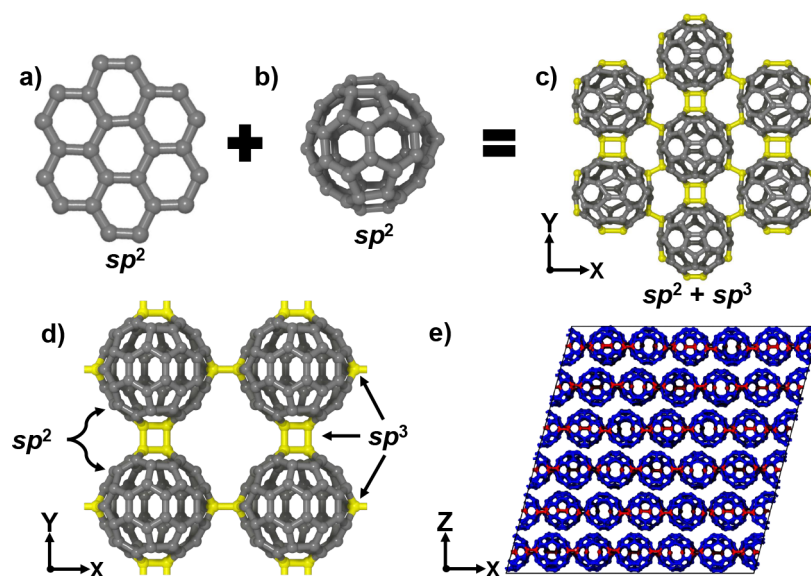
Figure 1. (a) The hexagonal structure of 2D graphene, (b) the 0D cage structure of a C_{60} molecule, (c) and the rhombohedral phase of polymerized C_{60} (dubbed graphullerite). Gray and yellow atoms/bonds correspond to sp^2- and sp^3-carbon, respectively. (d) The tetragonal phase of polymerized C_{60} where the fullerenes are polymerized in an orthogonal bonding orientation, which is different as compared to the hexagonal graphullerite structure. (e) Schematic of our computational domain for graphullerite, highlighting the layered structure.

mechanical strain and pressure.[13,14] Their thermal conductivity, however, has been shown to be on the opposite end of the spectrum (in comparison to graphene) with values <0.4 W m^{-1} K^{-1}.[7,9,10,15,16] This has been mainly attributed to the vibrational localization resulting from the weak nonbonded interactions.[6,8,15,17,18] Therefore, combining some of the exceptional physical properties of the different carbon allotropes in one material system could open the doors for engineering the next generation of fully organic, multifunctional materials potentially with large tunability in their physical properties. In this regard, incorporating C_{60} molecules in graphene-like sheets (with strong carbon−carbon bonds along the 2D sheets) that are stacked together to form a 3D structure (with nonbonded and relatively weaker interactions in the out-of-plane direction), such as in the case of graphullerite, could potentially offer the prospect of achieving highly anisotropic and potentially unrivaled physical properties in one material system.

Previously, polymerized phases of C_{60} have been synthesized through the application of extreme compression (>2.5 GPa) and high temperature (>500 K) conditions.[19−22] The 2D sheets of covalently bonded C_{60} molecules can display a rhombohedral bonding orientation (graphullerene),[1] as shown in Figure 1c, or a tetragonal bonding orientation (T-C_{60}),[23] as shown in Figure 1d. The fabrication of these polymerized carbon phases under ambient pressure conditions, as recently realized for graphullerene,[1,24] will facilitate a growing interest to incorporate these material systems in a plethora of applications such as in the next generation of battery materials and flexible electronics due to their relatively easier synthesis process that does not require extreme conditions. Therefore, a complete understanding of their physical properties is quintessential for their widespread use in such technologies.

In this work, we study the mechanical properties through uniaxial strain and thermal properties via nonequilibrium MD (NEMD) simulations of graphullerite. To understand the role of bond orientation in dictating the physical properties of polymerized fullerenes in general, we compare the results of

our graphullerite structure to a tetragonal structure with a different bonding orientation (see Figures 1c and 1d). We find that even along the 2D plane, the mechanical properties are highly anisotropic with the polymers showing a relatively stiffer response along the direction with two sp^3 bonds that are oriented parallel to the tensile axis (see Figure 1). Overall, as compared to T-C_{60}, graphullerite possesses higher bulk modulus ($B \sim 60$ GPa), Young's modulus ($E = 117−173$ GPa), and yield strength (~ 11 GPa). In terms of their thermal properties, we also observe anisotropy where these materials possess higher thermal conductivities along the direction parallel to the orientation of the double intermolecular bonds. However, in comparison to T-C_{60}, the graphullerite structure shows a drastically different temperature dependence where the thermal conductivity converges at higher temperatures along the two different directions with varying bond orientations. Overall, as compared to fullerite, the polymerized phases can demonstrate thermal conductivities that are higher than a factor of 30 at room temperature. These results highlight the remarkably tunable physical properties of polymerized C_{60} based on their bonding environment. Our results should help guide the incorporation of polymerized C_{60} structures in various technologies such as in flexible electronic devices and battery electrodes.

■ METHODS

We utilize the Large-scale Atomic/Molecular Massively Parallel Simulator (LAMMPS)[25] package to conduct our MD simulations. Our uniaxial strain simulations are conducted using a reactive potential (ReaxFF) to model the interatomic interactions.[26] The specific reactive potential chosen has been developed specifically to simulate condensed carbon phases, and has been shown to accurately predict the density functional theory (DFT)-based energies of a variety of fullerene structures.[27] The lattice constants predicted by the reactive potential can accurately replicate the experimentally determined values (details in the Supporting Information), thus validating our use of the potential to study the physical

properties of these polymers. We use a time step of 0.5 fs and periodic boundaries for all of our simulations.

Initially, our structures are relaxed under the NPT ensemble (with the number of atoms, pressure, and temperature held constant) for a total of 2 ns at the prescribed temperature. We assess the mechanical properties through uniaxial tensile deformation simulations along the in-plane (x- and y-) directions with a strain rate of 0.05 ns^{-1}. Throughout the tensile strain simulations, we prescribe "stress-free" conditions (with 0 bar pressure) along the orthogonal directions with the NPT integration. To generate stress−strain relationships for our C_{60} polymers, we calculate the applied strain and the resulting stress along that direction for every 0.1 ps during the simulation.

We also study the electronic properties of our polymerized fullerene structures by calculating the electronic band gaps and electron localization functions by performing DFT calculations with the QUANTUM ESPRESSO package.[28] For this, we utilize the Perdew−Burke−Ernzerhof exchange correlation functional to perform self-consistent field (SCF) calculations, while implementing the projector augmented wave pseudopotential for the carbon atoms. For all our SCF calculations, we use a plane wave basis with 50 Ry cutoff.

To predict the thermal conductivities of our polymerized structures, the NEMD method is used by utilizing the polymer consistent force field (PCFF) potential. Since NEMD simulations require very large computational domains,[29−31] the use of ReaxFF potential becomes computationally infeasible to predict the thermal conductivity. Therefore, we utilize the PCFF potential, which has been used to study the thermal properties of fullerene-based solids in prior literature.[6,8,15,17] Our NEMD approach utilizes Fourier's law to calculate the thermal conductivity via

$$Q = -\kappa \frac{dT}{dx} \tag{1}$$

where Q is the heat flux, κ is the thermal conductivity, and dT/dx is the temperature gradient in the direction of the applied heat flux. In this method, the simulation domain is extended along the direction of the applied heat flux, and a heat bath and a heat sink are established at opposite ends. A constant amount of energy is added and subtracted from the heat bath and heat sink, respectively, and a steady-state temperature gradient is established along the structure. The entire simulation domain is split in equal sized bins along the direction of the applied heat flux, and the temperatures of the atoms within each bin are averaged and used for calculations of the temperature gradient. An example of our NEMD simulation domain and the obtained temperature gradient are shown in Figure S1. Additional details of our NEMD simulations are given in the Supporting Information.

■ RESULTS AND DISCUSSIONS

The anisotropic mechanical properties obtained from our uniaxial tensile strain simulations on polymerized fullerenes described by the ReaxFF potential[27] are summarized in Figures 2a and 2b showing the stress−strain relationships in the two principle directions for unit cells of our graphullerite and T-C_{60} structures, respectively. For graphullerite, brittle fracture occurs when strained in both the x- and y-directions at strain levels of 10% and 6%, respectively. The Young's modulus is anisotropic, with values of 117 and 173 GPa in the x- and y-directions, respectively. Although the fracture strain for T-C_{60} is similar to
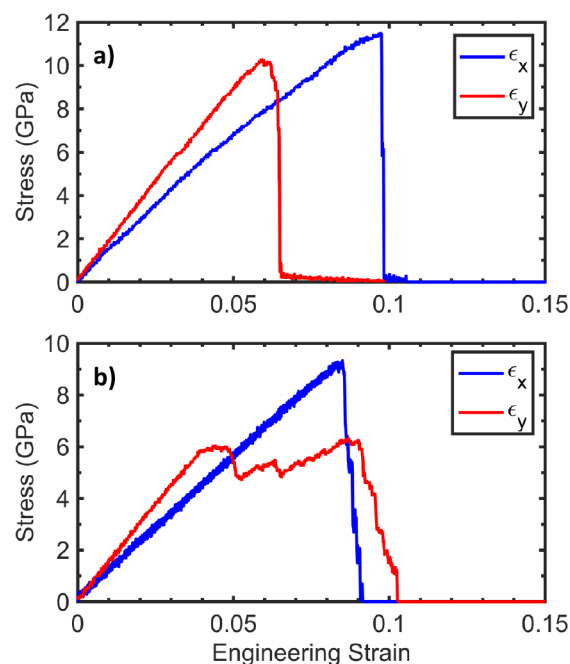

Figure 2. Stress−strain relationships for unit cells of our (a) graphullerite and (b) T-C_{60} structures under uniaxial tension. Significant plastic deformation behavior is seen for our T-C_{60} structure when uniaxial strain is applied in the y-direction.

graphullerite, the Young's modulus is lower in both directions; the Young's modulus of graphullerite is 25% larger than T-C_{60} in the double-bonded direction, signifying the important role played by the intermolecular bond environment in dictating their mechanical strength. However, these values are significantly lower in comparison to other 2D carbon allotropes such as graphene (~1 TPa),[4] graphyne (~600 GPa),[32] and penta-graphene (~260 GPa),[33] highlighting the highly flexible nature of the graphullerite structure (see Table 1).

Since polymerized C_{60} are sought after for future electrode materials, we also compare their mechanical properties to that of other (currently used) electrode materials in Table 1. The Young's modulus of graphullerite is comparable to that of the current rechargeable battery electrodes, with Young's moduli ranging from 124 to 264 GPa.[34] Similarly, we calculate the bulk modulus of graphullerite to be 60.9 GPa at room temperature, which is significantly lower than graphite (a similar layered structure), and also lower in comparison to other battery electrodes.[34] Again, this emphasizes the flexible nature of these polymerized carbon allotropes.

Another aspect worth noting from the stress−strain relationship of our T-C_{60} structure as shown in Figure 2b is the considerable plastic deformation that occurs under uniaxial strain along the y-direction (where the stress in the material does not change significantly while the material undergoes tensile deformation beyond the yield strength). In fact, larger supercell structures of both the graphullerite and T-C_{60} structures demonstrate this plastic deformation response along the y-direction, as shown in Figure 3. This plastic behavior originates from the partial breakage of bonds under an applied uniaxial strain, resulting in a "zipper-like" behavior in graphullerite (Figure 3c and d) in which a gradual breaking of bonds occurs along both principal directions. As the single bonds within the graphullerite structure are at a 30° angle to

Table 1. Mechanical, Thermal, and Electronic Properties of Our Graphullerite and T-C$_{60}$ Structures As Compared to Fullerite, Graphite, and Other Battery Electrode Materials

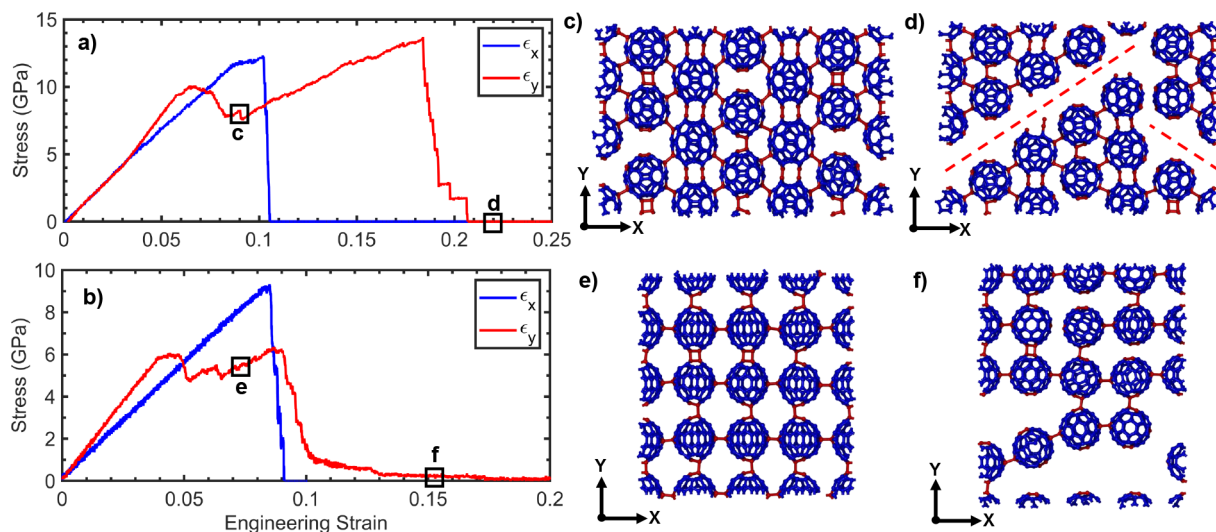| Material	Bulk modulus, B (GPa)	Young's modulus, E (GPa)	Yield strength, σ (GPa)	Thermal conductivity, κ (W m^{-1} K^{-1})	Band gap (eV)
Graphullerite	60.9	$E_x = 117.4$	$\sigma_x = 11.4$	$\kappa_x = 10.6$	0.54
		$E_y = 172.7$	$\sigma_y = 10.2$	$\kappa_y = 13.3$	
T-C$_{60}$	38.6	$E_x = 109.6$	$\sigma_x = 9.3$	$\kappa_x = 5.8$	-
		$E_y = 128.9$	$\sigma_y = 6.0$	$\kappa_y = 12.1$	
Fullerite	7.21	-	-	0.44	1.5 [35]
Graphite	227	1400	160	2000	0.04 [36]
LiCoO$_2$	163 [34]	264 [34]	-	3.7−5.4 [37]	0.94 [38]
LiFePO$_4$	93.9 [39]	124 [39]	-	0.39 [40]	0.2 [41]
LiMn$_2$O$_4$	133 [34]	194 [34]	-	0.99 [40]	0.92 [42]

Figure 3. Stress−strain relationships of our (a) graphullerite and (b) T-C$_{60}$ bulk structures under applied uniaxial strains in the x- (blue line) and y- (red line) directions. (c, d) Snapshots of our graphullerite structure under various strain levels in the y-direction as shown in a. (c) When strained in the y-direction, plastic deformation initiates at a strain of ∼6%, where both the single sp^3 and double sp^3 bonds are broken. (d) This behavior persists at higher strains, resulting in a brittle fracture at a strain of ∼20% where fracture lines form at ∼30° angles relative to the x-direction, rather than perpendicular to the applied strain. (e, f) Snapshots of our T-C$_{60}$ structure under various strain levels as shown in b. (e) When strained in the y-direction, plastic deformation initiates at ∼4% strain, where approximately half of each sp^3 intermolecular bonds parallel to the applied strain are broken. (f) At a strain of ∼9%, a nonbrittle fracture occurs, where the bonds perpendicular to the applied strain are broken which is in contrast to the failure mechanism in our graphullerite structure.

the x-direction, these bonds can participate in the distribution of stress and break individually when uniaxial strain is applied in the y-direction. In comparison, the single bonds within the T-C$_{60}$ structure that are parallel with the x-direction do not participate in the distribution of stress when uniaxial strain is applied along the y-direction. Instead, double bonds aligned in the y-direction of our T-C$_{60}$ structure break individually (see Figure 3e and f), causing a slight reorientation of the fullerene cages before fracturing completely at higher strain levels. For both of our supercell structures, when uniaxial strain is applied along the x-direction, a brittle fracture occurs in which the intermolecular bonds aligned in the x-direction break, with each layer fracturing independently of each other. Note, this unique strain response of the supercells is in contrast to the brittle fracture that we observe in a similarly layered graphite structure described by the same ReaxFF potential (Figure S7).

Before we examine the vibrational thermal properties, we gauge the semiconducting nature of these materials through density functional theory (DFT) calculations. We find a band gap of 0.54 eV for graphullerite, which confirms that the electronic subsystem has negligible influence in dictating their thermal behavior. Furthermore, we also investigate the effect of

uniaxial strain on their electronic structure by calculating and visualizing the charge densities through contour plots of the electron localization function. The charge density contour illustrates the spatial distribution of electron density surrounding the bonds within a range of 0 to 1, where the two extremes, 0 (blue) and 1 (red) represent no bonds and strong covalent bonds, respectively. For the graphullerite structure at a 0% strain level, we predict the presence of intermolecular covalent bonds, as evidenced by the high electron localization between fullerene molecules (Figure 4a). However, the application of strain results in a more delocalized nature of the charge densities as evidenced by the larger spatial overlaps from the covalent intermolecular bonds and intramolecular bonds within the fullerene cages, as visualized in Figure 4b at a 4% strain level. This delocalization also leads to the reduction of the band gap to ∼0.3 eV for strain levels near the fracture limit. For the unstrained T-C$_{60}$, we find that the single C−C bonds aligned in the x-direction disappear as shown in Figure S9a, and the structure becomes a series of 1D chains oriented along the y-direction. As such, we do not calculate the electronic band gap for the T-C$_{60}$ structure.
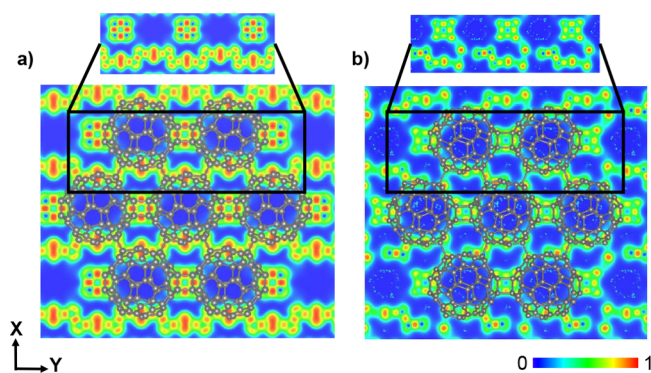
Figure 4. Contour plots of charge density for graphullerite under (a) unstrained condition and (b) for 4% uniaxial strain along the *x*-direction. (top panel). The localized electron density of graphullerite exhibits noticeable delocalization under uniaxial strain as highlighted in the top panels.

Next, we investigate the thermal properties of our polymerized fullerene structures by utilizing the NEMD method to calculate their temperature-dependent thermal conductivities along the two principal bonded directions. Figure 5a and b shows the results of our calculations for the graphullerite and the T-C_{60} structures, respectively. For comparison, we also plot the thermal conductivity of fullerite.[31] Our results show that the polymerization of the fullerene molecules can result inasmuch as a 30× increase in the thermal conductivity as compared to the nonbonded fullerite at room temperature. We attribute this mainly to the introduction of additional heat carrying vibrational modes in the 2−7 THz regime, owing to the intermolecular bonds between fullerene molecules, as shown by our vibrational density of states (DOS) calculations for all three structures in Figure 5c. Additional modes are also introduced at higher frequencies, which can also provide additional channels of heat conduction for the polymerized phases. Furthermore, the thermal conductivity of ∼13 W m^{-1} K^{-1} of graphullerite is ∼2−3× higher than the thermal conductivities of currently used electrodes such as $LiCoO_2$, $LiFePO_4$, and $LiMn_2O_4$, as listed in Table 1. The anisotropic nature of our structures in the in-plane versus cross-plane direction is also present in these same battery electrode materials. In these materials, the van der Waals gap is necessary to facilitate the diffusion of ions into and out of the material, which can result in dramatic changes in the thermal conductivity in the cross-plane direction.[43,44] This highlights the applicability of these materials as high thermal conductivity electrodes, which could potentially lead to better thermal management and prevention of thermal runaway in rechargeable batteries.[45] However, due to their high thermal conductivities in the in-plane directions, these materials are unfeasible for applications such as in thermoelectric devices where low lattice thermal conductivities are desirable.

We also find that uniaxial strain has a negligible influence on the thermal conductivity in all directions for both our graphullerite and T-C_{60} structures (Figure 5d). In general, for inorganic crystals, uniaxial tension usually results in a reduction in thermal conductivity along the direction of the applied strain. However, for these polymers, the negligible influence of uniaxial strain (before catastrophic failure of the structures) on the thermal conductivity again emphasizes their flexible nature and the ability to retain their physical properties even under strained conditions.

Our polymerized structures exhibit a large degree of anisotropy in their in-plane thermal conductivities owing to the varying bonding orientation along the two principal directions. However, this anisotropy is reduced for graphullerite at higher temperatures. This mainly results from the varying vibrational scattering mechanisms responsible in dictating the temperature dependence of thermal conductivity along the two orthogonal directions. More specifically, along the double-bonded (*y*-) direction, Umklapp scattering dominated anharmonic processes drive the reduction in thermal conductivity as temperature is increased. This is evidenced by the near $1/T$ temperature dependence in that direction (Figure 5a). However, along the *x*-direction where the single bonds are oriented at ∼30° to the principal axis, anharmonic processes have a lesser influence in dictating the temperature dependence as evidenced by $\kappa \propto 1/T^{0.4}$ in that direction. In contrast, the temperature-dependent thermal conductivities along the two principal (in-plane) directions in the T-C_{60} structure show similar trends owing to the perfectly oriented bonds along the direction of the principal axes. Along the double-bonded (*y*-) direction, however, the thermal conductivities are higher for the entire temperature range (in contrast to the temperature dependence of the graphullerite structure). These results highlight the importance of bonding environment in dictating the temperature-dependent thermal conductivity in the polymerized phases and provides an avenue to manipulate their vibrational thermal transport by carefully varying the bonding orientation. Once fracture occurs in these structures, the thermal conductivity is reduced significantly due to the breaking of intermolecular bonds between fullerene molecules as shown in Figure 5d.

We note that the temperature dependencies of our polymerized fullerenes are drastically different than the fullerite structure (see Figure 5a and b). For our fullerite, we observe a more crystal-like temperature dependence for the low temperature regime, while we obtain a temperature-independent thermal conductivity at higher temperatures (>150 K). Earlier works have ascribed this unique temperature dependence to vibrational scattering at higher temperatures induced by the librational and rotational motion of the fullerene molecules.[17,46,47] Specifically, at high temperatures, the molecules (held together by weak van der Waals forces) acquire enough kinetic energy to overcome the energy barrier between the local energy minima and perform free rotations. This causes the scattering of the heat carrying vibrations, resulting in the amorphous-like temperature dependence (or the lack thereof) for fullerites. In contrast, as discussed above, the temperature dependence of our polymerized phases largely show a crystalline-like behavior, which can be manipulated by the bonding orientation.

■ CONCLUSIONS

In summary, we provide atomistic-level insights into the mechanical and thermal properties of a newly synthesized allotrope of carbon formed via the polymerization of C_{60} in a hexagonal lattice (similar to graphite) and dubbed graphullerite. The introduction of covalent intermolecular bonds in the polymerization process endows these structures with remarkable flexibility and high thermal conductivities. These physical attributes depend largely on the bond orientation where higher thermal conductivity and Young's modulus are associated with directions that have preferentially oriented double covalent bonds along that direction. Furthermore, in
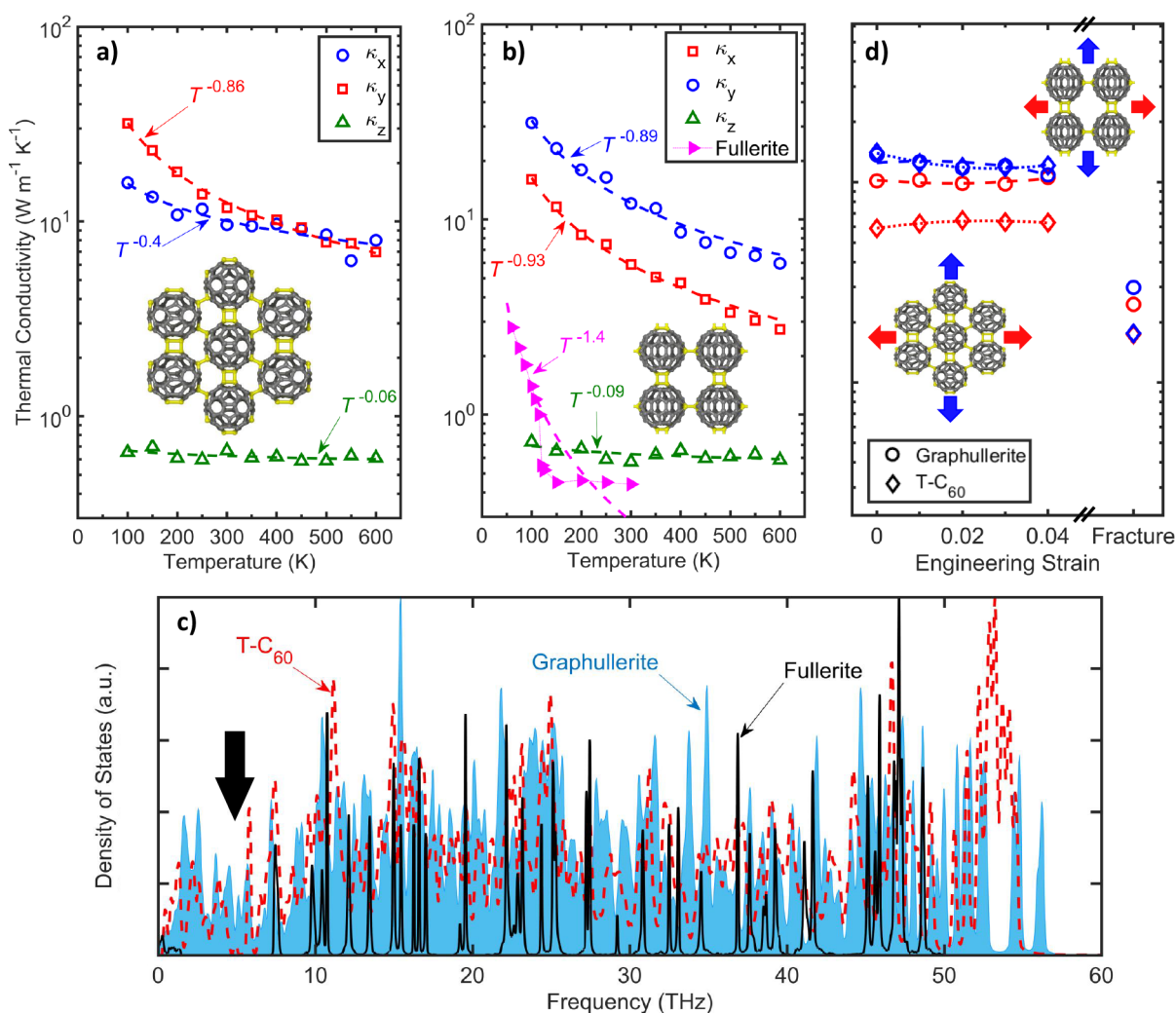
Figure 5. Temperature-dependent thermal conductivities for our (a) graphullerite and (b) T-C_{60} structures. The thermal conductivity of a face centered cubic fullerite structure is also shown for comparison. Part of the data have been adapted in part with permission from our earlier works in refs 31 and ref 1. Copyright 2022 American Chemical Society, and 2023 Springer Nature, respectively. At low temperatures, the thermal conductivity of graphullerite is highly anisotropic, but becomes less so at higher temperatures due to the reduced temperature dependence of κ_x. In contrast, the T-C_{60} structure remains highly anisotropic over the temperature range investigated. For both structures, the thermal conductivity can be increased by as much as ~30× when compared to the fullerite structure. (c) Vibrational density of states for graphullerite, T-C_{60}, and fullerite structures. Additional heat carrying vibrational modes are introduced in the 2−7 THz regime due to the introduction of intermolecular bonds between the fullerenes in the polymerized phases. (d) Strain-dependent thermal conductivity for our graphullerite (circle) and T-C_{60} (diamond) structures in the x- (red) and y- (blue) directions. Application of uniaxial strain does not significantly affect the thermal conductivity in the range of strains investigated. Once fracture occurs, the thermal conductivity in the direction of applied strain is drastically reduced.

contrast to the brittle fracture in graphite resulting from uniaxial strain, considerable plastic deformation occurs for these polymerized C_{60} phases, which we attribute to the sequential breaking of the sp^3 bonds under the application of tensile strains beyond the elastic regime. Our DFT-based calculations show that graphullerite has a band gap of 0.54 eV, which decreases due to the application of uniaxial strain and the concomitant delocalization of the electron densities. The anisotropy in the vibrational thermal transport in these semiconductors also greatly depends on the bonding orientation, which can be utilized to control the relative contributions from anharmonic phonon−phonon scattering and vibrational scattering due to bonding heterogeneity in these polymerized phases of fullerenes. Our results highlight the remarkable anisotropic physical properties of graphullerite, which could be beneficial for applications such as in the next

generation of energy storage and flexible optoelectronic devices.

■ ASSOCIATED CONTENT

ⓢ Supporting Information

The Supporting Information is available free of charge at https://pubs.acs.org/doi/10.1021/acsomega.3c01412.

> Details of reactive potential validation, strain simulations, bulk modulus calculations, thermal conductivity calculations, and T-C_{60} electronic structure calculations (PDF)

■ AUTHOR INFORMATION

Corresponding Author

Ashutosh Giri − *Department of Mechanical, Industrial and Systems Engineering, University of Rhode Island, Kingston,*

Rhode Island 02881, United States; ● orcid.org/0000-0002-8899-4964; Email: ashgiri@uri.edu

Authors

Connor Jaymes Dionne − *Department of Mechanical, Industrial and Systems Engineering, University of Rhode Island, Kingston, Rhode Island 02881, United States;* ● orcid.org/0000-0002-1539-1601

Muhammad Akif Rahman − *Department of Mechanical, Industrial and Systems Engineering, University of Rhode Island, Kingston, Rhode Island 02881, United States*

Complete contact information is available at:
https://pubs.acs.org/10.1021/acsomega.3c01412

Author Contributions

C. Jaymes Dionne: Conceptualization, Molecular dynamics simulations, Investigation, Formal analysis, Validation, Writing. **Muhammad Akif Rahman**: Density functional theory calculations. **Ashutosh Giri**: Conceptualization, Methodology, Writing - Review & Editing, Supervision, Project administration, Funding acquisition.

Notes

The authors declare no competing financial interest.

■ REFERENCES

(1) Meirzadeh, E.; Evans, A.; Rezaee, M.; Milich, M.; Dionne, C. J.; Darlington, T. P.; Bao, S. T.; Bartholomew, A. K.; Handa, T.; Rizzo, D. J.; et al. A few-layer covalent network of fullerenes. *Nature* **2023**, *613*, 71−76.

(2) Ando, T. The electronic properties of graphene and carbon nanotubes. *NPG Asia Materials* **2009**, *1*, 17−21.

(3) Castro Neto, A. H.; Guinea, F.; Peres, N. M. R.; Novoselov, K. S.; Geim, A. K. The electronic properties of graphene. *Rev. Mod. Phys.* **2009**, *81*, 109−162.

(4) Lee, C.; Wei, X.; Kysar, J. W.; Hone, J. Measurement of the Elastic Properties and Intrinsic Strength of Monolayer Graphene. *Science* **2008**, *321*, 385−388.

(5) Balandin, A. A.; Ghosh, S.; Bao, W.; Calizo, I.; Teweldebrhan, D.; Miao, F.; Lau, C. N. Superior Thermal Conductivity of Single-Layer Graphene. *Nano Lett.* **2008**, *8*, 902−907.

(6) Giri, A.; Hopkins, P. E. Spectral Contributions to the Thermal Conductivity of C60 and the Fullerene Derivative PCBM. *J. Phys. Chem. Lett.* **2017**, *8*, 2153−2157.

(7) Olson, J. R.; Topp, K. A.; Pohl, R. O. Specific Heat and Thermal Conductivity of Solid Fullerenes. *Science* **1993**, *259*, 1145−1148.

(8) Giri, A.; Hopkins, P. E. Pronounced low-frequency vibrational thermal transport in C60 fullerite realized through pressure-dependent molecular dynamics simulations. *Phys. Rev. B* **2017**, *96*, 220303.

(9) Liang, Q.; Bartnof, M.; He, Y.-L.; Malen, J. A.; McGaughey, A. J. H. Fullerene rotational dynamics generate disordered configurations that suppress thermal conductivity in superatomic crystals. *Nanoscale Horizons* **2020**, *5*, 1524−1529.

(10) Wang, X.; Liman, C. D.; Treat, N. D.; Chabinyc, M. L.; Cahill, D. G. Ultralow thermal conductivity of fullerene derivatives. *Phys. Rev. B* **2013**, *88*, 075310.

(11) Laranjeira, J.; Marques, L. C60 structures: Structural, electronic and elastic properties. *Materials Today Communications* **2020**, *23*, 100906.

(12) Ruoff, R. S.; Ruoff, A. L. The bulk modulus of C60 molecules and crystals: A molecular mechanics approach. *Appl. Phys. Lett.* **1991**, *59*, 1553−1555.

(13) Berdinsky, A. S.; Fink, D.; Gridchin, V. A.; Petrov, A. V. Conductivity of fullerite structures under different types of pressure. *7th International Conference on Actual Problems of Electronic Instrument Engineering Proceedings, 2004*; IEEE: Piscataway, NJ, 2004; pp 2−9.

(14) Hansen, P.; Fallon, P.; Krätschmer, W. An EELS study of fullerite — C60/C70. *Chem. Phys. Lett.* **1991**, *181*, 367−372.

(15) Giri, A.; Chou, S. S.; Drury, D. E.; Tomko, K. Q.; Olson, D.; Gaskins, J. T.; Kaehr, B.; Hopkins, P. E. Molecular tail chemistry controls thermal transport in fullerene films. *Phys. Rev. Materials* **2020**, *4*, 065404.

(16) Duda, J. C.; Hopkins, P. E.; Shen, Y.; Gupta, M. C. Exceptionally low thermal conductivities of films of the fullerene derivative PCBM. *Phys. Rev. Lett.* **2013**, *110*, 015902.

(17) Kumar, S.; Shao, C.; Lu, S.; McGaughey, A. J. H. Contributions of different degrees of freedom to thermal transport in the C60 molecular crystal. *Phys. Rev. B* **2018**, *97*, 104303.

(18) Szwejkowski, C. J.; Giri, A.; Warzoha, R.; Donovan, B. F.; Kaehr, B.; Hopkins, P. E. Molecular Tuning of the Vibrational Thermal Transport Mechanisms in Fullerene Derivative Solutions. *ACS Nano* **2017**, *11*, 1389−1396.

(19) Chen, X.; Yamanaka, S.; Sako, K.; Inoue, Y.; Yasukawa, M. First single-crystal X-ray structural refinement of the rhombohedral C60 polymer. *Chem. Phys. Lett.* **2002**, *356*, 291−297.

(20) Chen, X.; Yamanaka, S. Single-crystal X-ray structural refinement of the 'tetragonal' C60 polymer. *Chem. Phys. Lett.* **2002**, *360*, 501−508.

(21) Yamanaka, S.; Kubo, A.; Inumaru, K.; Komaguchi, K.; Kini, N. S.; Inoue, T.; Irifune, T. Electron conductive three-dimensional polymer of cuboidal C60. *Physical review letters* **2006**, *96*, 076602.

(22) Alvarez, M.; Hodeau, J. L. Structural phase transitions of C60 under high-pressure and high-temperature. *Carbon* **2015**, *82*, 381−407.

(23) Tanaka, M.; Yamanaka, S. Vapor-Phase Growth and Structural Characterization of Single Crystals of Magnesium Doped Two-Dimensional Fullerene Polymer Mg2C60. *Cryst. Growth Des.* **2018**, *18*, 3877−3882.

(24) Hou, L.; Cui, X.; Guan, B.; Wang, S.; Li, R.; Liu, Y.; Zhu, D.; Zheng, J. Synthesis of a monolayer fullerene network. *Nature* **2022**, *606*, 507−510.

(25) Plimpton, S. Fast Parallel Algorithms for Short-Range Molecular Dynamics. *J. Comput. Phys.* **1995**, *117*, 1−19.

(26) van Duin, A. C. T.; Dasgupta, S.; Lorant, F.; Goddard, W. A. ReaxFF:Äâ A Reactive Force Field for Hydrocarbons. *J. Phys. Chem. A* **2001**, *105*, 9396−9409.

(27) Srinivasan, S. G.; van Duin, A. C. T.; Ganesh, P. Development of a ReaxFF Potential for Carbon Condensed Phases and Its Application to the Thermal Fragmentation of a Large Fullerene. *J. Phys. Chem. A* **2015**, *119*, 571−580.

(28) Giannozzi, P.; Baroni, S.; Bonini, N.; Calandra, M.; Car, R.; Cavazzoni, C.; Ceresoli, D.; Chiarotti, G. L.; Cococcioni, M.; Dabo, I.; et al. QUANTUM ESPRESSO: a modular and open-source software project for quantum simulations of materials. *J. Phys.: Condens. Matter* **2009**, *21*, 395502.

(29) Sellan, D. P.; Landry, E. S.; Turney, J. E.; McGaughey, A. J. H.; Amon, C. H. Size effects in molecular dynamics thermal conductivity predictions. *Phys. Rev. B* **2010**, *81*, 214305.

(30) Schelling, P. K.; Phillpot, S. R.; Keblinski, P. Comparison of atomic-level simulation methods for computing thermal conductivity. *Phys. Rev. B* **2002**, *65*, 144306.

(31) Dionne, C. J.; Giri, A. Magnesium Doping Enhances Thermal Conductivity of Polymerized Fullerene Crystals. *J. Phys. Chem. C* **2022**, *126*, 17406−17414.

(32) Zou, B.; Shen, J.; Yu, P.; Zhao, J. The Young's moduli of three types of carbon allotropes: a molecular mechanics model and a finite-element method. *Proceedings. Mathematical, Physical, And Engineering Sciences* **2016**, *472*, 20150628.

(33) Zhang, S.; Zhou, J.; Wang, Q.; Chen, X.; Kawazoe, Y.; Jena, P. Penta-graphene: A new carbon allotrope. *Proc. Natl. Acad. Sci. U. S. A.* **2015**, *112*, 2372−2377.

(34) Qi, Y.; Hector, L. G.; James, C.; Kim, K. J. Lithium Concentration Dependent Elastic Properties of Battery Electrode Materials from First Principles Calculations. *J. Electrochem. Soc.* **2014**, *161*, F3010−F3018.

(35) Saito, S.; Oshiyama, A. Cohesive mechanism and energy bands of solid C60. *Phys. Rev. Lett.* **1991**, *66*, 2637−2640.

(36) Partoens, B.; Peeters, F. M. From graphene to graphite: Electronic structure around the K point. *Phys. Rev. B* **2006**, *74*, 075404.

(37) Cho, J.; Losego, M. D.; Zhang, H. G.; Kim, H.; Zuo, J.; Petrov, I.; Cahill, D. G.; Braun, P. V. Electrochemically tunable thermal conductivity of lithium cobalt oxide. *Nat. Commun.* **2014**, *5*, 4035.

(38) Santana, J.; Kim, J.; Kent, P.; Reboredo, F. Successes and failures of Hubbard-corrected density functional theory: The case of Mg doped LiCoO2. *J. Chem. Phys.* **2014**, *141*, 164706.

(39) Maxisch, T.; Ceder, G. Elastic properties of olivine LiFePO4 from first principles. *Phys. Rev. B* **2006**, *73*, 174112.

(40) Richter, F.; Kjelstrup, S.; Vie, P. J. S.; Burheim, O. S. Thermal conductivity and internal temperature profiles of Li-ion secondary batteries. *J. Power Sources* **2017**, *359*, 592−600.

(41) Zhou, F.; Kang, K.; Maxisch, T.; Ceder, G.; Morgan, D. The electronic structure and band gap of LiFePO4 and LiMnPO4. *Solid State Commun.* **2004**, *132*, 181−186.

(42) Chakraborty, A.; Dixit, M.; Aurbach, D.; Major, D. T. Predicting accurate cathode properties of layered oxide materials using the SCAN meta-GGA density functional. *npj Computational Materials* **2018**, *4*, 60.

(43) Cho, J.; Losego, M. D.; Zhang, H. G.; Kim, H.; Zuo, J.; Petrov, I.; Cahill, D. G.; Braun, P. V. Electrochemically tunable thermal conductivity of lithium cobalt oxide. *Nat. Commun.* **2014**, *5*, 4035.

(44) Qian, X.; Gu, X.; Dresselhaus, M. S.; Yang, R. Anisotropic Tuning of Graphite Thermal Conductivity by Lithium Intercalation. *J. Phys. Chem. Lett.* **2016**, *7*, 4744−4750.

(45) Kantharaj, R.; Marconnet, A. M. Heat Generation and Thermal Transport in Lithium-Ion Batteries: A Scale-Bridging Perspective. *Nanoscale and Microscale Thermophysical Engineering* **2019**, *23*, 128−156.

(46) Giri, A.; Hopkins, P. E. Spectral Contributions to the Thermal Conductivity of C60 and the Fullerene Derivative PCBM. *J. Phys. Chem. Lett.* **2017**, *8*, 2153−2157.

(47) Chen, L.; Wang, X.; Kumar, S. Thermal Transport in Fullerene Derivatives Using Molecular Dynamics Simulations. *Sci. Rep.* **2015**, *5*, 12763.